NUMERICAL MODELING OF IRREGULAR WAVE ON MUD LAYER USING SPECTRAL METHOD

Kourosh Hejazi[1], Saeideh Sami[1], Mohsen Soltanpour[1] and Farzin Samsami[1]

Irregular wave propagation in a combined system of water and mud layer has been investigated by using a laterally averaged finite volume numerical model and spectral method. The fully non-linear Navier-Stokes equations based on ALE description with kinematic and dynamic boundary conditions at free surface and interface together with the Bingham constitutive equation for modeling the behavior of mud layer are solved in the numerical model. The application of the model for hydrodynamic tests including a periodic progressive wave over a submerged bar and the irregular wave propagation, shows the ability of the numerical model in prediction of water surface elevation and wave spectrum shape. For irregular wave-mud interaction test, variations of the spectral characteristics of different type of wave spectra have been considered. In spite of discrepancies between predicted and measured results, the accuracy of the predictions for attenuated irregular waves is acceptable.

Keywords: irregular wave-mud interaction; spectral method; Bingham equation; projection method; ALE description

INTRODUCTION

Wave attenuation and mud mass transport are two noteworthy phenomena of wave-mud interaction, which have been observed both at laboratory and in field when waves propagate over a muddy bottom (Zhang and Zhao 1999). Real conditions of the muddy coasts suggest the irregularity of the natural waves as an important factor to be investigated. At present, five methods are available to deal with the transformation and action of random sea waves including significant wave representation method, highest wave representation method, probability calculation method, irregular wave test method, and spectral calculation method (Goda 2000). In the spectral method, an irregular wave can be seen as the linear superposition of a series of sinusoidal waves, each with its own frequency, amplitude and phase in the frequency domain. The study of the frequency characteristics of such an irregular wave may be accomplished by the use of Fourier series analysis. A few researchers have considered the irregularity of water waves using spectral calculations for numerical simulations. A multi-layer hydrodynamic model in addition to a proposed rheological equation has been presented by Zhang and Zhao (1999) to analytically investigate regular and irregular waves based on a repetitive method or through a trial and error method. They firstly took a representative wave with the height of the significant wave and the frequency of peak spectra and calculated the rheological parameters by the interaction of the representative wave with mud bed through the multi-layer model. After modeling the measured wave spectra of the base point by component wave method, wave damping of all component waves was then calculated using these rheological parameters and finally the wave spectra at all points was obtained. The total mass transport velocity due to irregular waves was computed as the sum of each component wave. Multi-layered water-fluid mud model with the constitutive equations of visco-elastic-plastic model of Soltanpour et al. (2007) uses three methods of representative wave, statistical analysis and spectral method to model irregular waves and mud mass transport. Different definitions of the representative wave, i.e. mean wave, significant wave and root-mean-square were examined. De Boer et al. (2009) performed a series of experiments in order to investigate regular and irregular wave damping due to the presence of the fluid mud. The results showed that the waves experienced a frequency-dependent damping rate that were in agreement with dispersion relation of Kranenburg (2008). It was also showed that wave-wave interactions were significant, especially at shorter peak period in the JOWNSWAP spectrum. Recently Samsami (2012) conducted a series of wave flume experiments to investigate irregular wave-mud interaction with different type of incident wave spectra, in presence of a current and without it.

In this study the interaction between irregular wave with a muddy bed has been investigated by a laterally averaged numerical model. The numerical model is based on the fully nonlinear Navier-Stokes equations and the complete set of the non-linear free surface and interface boundary conditions. The model includes the constitutive equation of Bingham plastic for mud layer, which its accuracy in simulating the propagation of regular waves over a viscous fluid mud layer has been evaluated satisfactorily (Hejazi et al. 2013). For application of irregular waves the spectral method has been

[1] Civil Engineering Department, K.N. Toosi University of Technology, No.1346, Vali-Asr Ave., Tehran, P.C. 1996715433, Iran

utilized. The wave height attenuation and the changes of wave spectral shape along the fluid mud layer have been considered. The irregular wave was generated using the parameterized JONSWAP, Pierson-Moskowitz, and Neumann spectra at the inlet boundary. Comparison of the predicted values with the experimental data confirms the capability of the model in effective simulation of irregular wave attenuation.

GOVERNING EQUATIONS

The problem of interest in the present study is shown in Fig. 1. The upper layer is plain water subject to a wave disturbance, $\eta_w(x,t)$, and the lower layer is fluid mud bounded below by a rigid plane at $z = z_b(x)$.

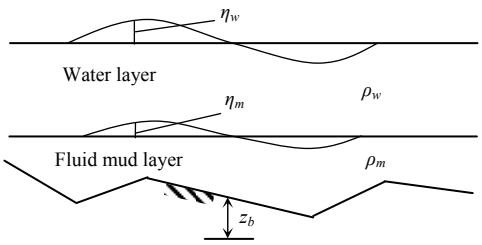

Figure 1. Schematic diagram of the two-layer viscous fluid system in the 2DV presentation.

The governing equations for both water and the mud are the continuity equation and the equations of motion for incompressible fluids. The conservative form of equations in ALE (arbitrary Lagrangian-Eulerian) description may be expressed as follows:

$$\frac{\partial u_i}{\partial x_i} = 0 \tag{1}$$

$$\frac{\partial u_i}{\partial t} + \frac{\partial u_i u_j}{\partial x_j} - u_g \frac{\partial u_i}{\partial x_j} = -\frac{\rho_r}{\rho}\frac{\partial P}{\partial x_i} + \frac{1}{\rho}\frac{\partial \tau_{ij}}{\partial x_j} - \left(\frac{\rho - \rho_r}{\rho}\right) g \tag{2}$$

where t is time, x is the Cartesian coordinate, u is the velocity, P is the pressure in the absence of hydrostatic pressure divided by reference density of water, ρ is the fluid density, ρ_r is the reference density of water, τ is the symmetric extra-stress tensor, g is the gravitational acceleration, and u_g is the vertical mesh velocity obtained from the vertical displacement of mesh in each time step which only appears for $j = 2$. The indices $i, j = 1, 2$ represent the coordinate directions. The last term of Eq. 2 is only included for $i = 2$.

The relation between the stress tensor and the shear rate tensor, $\dot{\gamma}_{ij}$, for Newtonian fluids is expressed as follows:

$$\tau_{ij} = \mu \dot{\gamma}_{ij} \tag{3}$$

$$\dot{\gamma}_{ij} = \frac{\partial u_i}{\partial x_j} + \frac{\partial u_j}{\partial x_i} \tag{4}$$

where the viscosity, μ, is independent of shear rate tensor. Different constitutive equations have been assumed for prediction of the mud behavior. The model of ideal Bingham constitutive equations have been proposed as follows:

$$\begin{aligned} \tau_{ij} &= \tau_y + \mu_B \dot{\gamma}_{ij} \quad for \left|\tau_{ij}\right| > \tau_y \\ \dot{\gamma}_{ij} &= 0, \qquad\qquad for \left|\tau_{ij}\right| > \tau_y \end{aligned} \tag{5}$$

where τ_y is the yield stress, and μ_B is the plastic viscosity. To avoid the discontinuity inherent in this model at the yield point, $\tau = \tau_y$, Papanastasiou (1987) proposed a modified expression that lets the shear stress vary continuously with the shear rate according to Eq. 6:

$$\tau_{ij} = \tau_y \left[1 - \exp(-m\dot{\gamma}_{ij})\right] + \mu_B \dot{\gamma}_{ij} \tag{6}$$

where m is the material parameter. The ideal Bingham fluid can be closely approximated if m is large enough. Eq. 6 can be rewritten as follows:

$$\tau_{ij} = \left(\mu_B + \frac{\tau_y}{\left|\dot{\gamma}_{ij}\right|}\left[1 - \exp(-m\left|\dot{\gamma}_{ij}\right|)\right] \right) \dot{\gamma}_{ij} \tag{7}$$

where $\left|\dot{\gamma}_{ij}\right| = \sqrt{0.5 tr\, \dot{\gamma}_{ij}^2}$ is the second invariant of the rate-of-strain tensor. By substituting Eq. 7 in Eq.2, the momentum equations for the Bingham plastic fluid mud may be obtained as follows:

$$\begin{aligned} &\frac{\partial u_i}{\partial t} + \frac{\partial u_i u_j}{\partial x_j} - u_g \frac{\partial u_i}{\partial x_j} = \\ &-\frac{\rho_r}{\rho}\frac{\partial P}{\partial x_i} + \frac{1}{\rho}\frac{\partial}{\partial x_j}\left\{ \mu_B + \frac{\tau_y}{\left|\dot{\gamma}_{ij}\right|}\left[1 - \exp(-m\left|\dot{\gamma}_{ij}\right|)\right] \right\} - \left(\frac{\rho - \rho_r}{\rho} \right) g \end{aligned} \tag{8}$$

SPECTRAL METHOD

To conduct the analysis based on the spectral method, a time record segment containing many waves is selected. One assumption implicit in this analysis, is that the signal being studied repeats itself after each (long) interval. Wave records do not exhibit this characteristic exactly, but that is neglected for this analysis. The elevation of a long-crested irregular sea wave, propagating along the positive x axis, may be written as the sum of a large number of regular wave components as follows:

$$\eta(t) = \sum_{n=1}^{N} a_n \cos(k_n x - \omega_n t + \varepsilon_n) \tag{9}$$

in which, for each component, n, a_n is the wave amplitude component, ω_n is the circular frequency component, k_n is the wave number component and ε_n is the random phase angle component normally distributed over the range between 0 and 2π. The Fourier series thus yields a set of values for wave amplitude and the random phase angle, each associated with its own circular frequency. If enough Fourier series terms are included, the entire time record at a point may be reproduced using this set of values. The wave amplitude, a_n, may be expressed in a wave spectrum, $S(\omega_n)$ as:

$$S(\omega_n) \cdot \Delta\omega = \sum_{\omega_n}^{\omega_n + \Delta\omega} \frac{1}{2} a_n^2 \tag{10}$$

where $\Delta\omega$ is a constant difference between two successive frequencies. Multiplied with ρg, this expression is the energy per unit area of the waves in the frequency interval $\Delta\omega$ (Fig. 2).

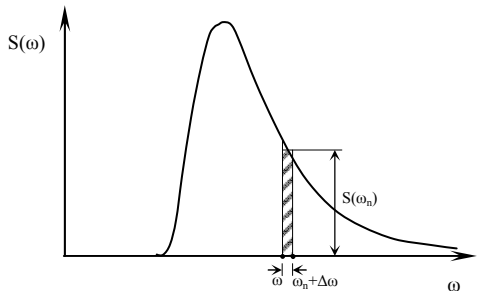

Figure 2. Definition of spectral density.

Letting $\Delta\omega \to 0$, the definition of the wave energy spectrum $S(\omega)$ becomes:

$$S(\omega_n) \cdot d\omega = \frac{1}{2} a_n^2 \tag{11}$$

or the wave energy spectra as a function of frequency in Hertz ($f = 1/T$) becomes:

$$S(f_n)\cdot df = \frac{1}{2}a_n^2 \tag{12}$$

A Fourier transform converts a signal in the time domain to the frequency domain (spectrum). The original and the newly obtained wave structure differ because different phase angles have been used. However, they contain an equal amount of energy and are statistically identical.

Relationships with statistics can be found from computing the moments of the area under the spectrum with respect to the vertical axis at $\omega \rightarrow 0$. If m denotes a moment, then m_n denotes the n^{th} order moment given in this case by:

$$m_n = \int_0^\infty S(f)\, f^n\, df, n = -1,0,1,2,\cdots \tag{13}$$

This means that m_0 is the area under the spectral curve, m_1 is the first order moment (static moment) of this area and m_2 is the second order moment (moment of inertia) of this area. m_0 is an indication of the variance squared, of the water surface elevation. Of course this m_0 can also be related to the various wave amplitudes and heights. The significant wave height, H_{m_0}, the root mean square wave height, H_{rms}, and the highest one-tenth wave height, $H_{1/10}$, are respectively calculated by the Eq. 14 as follows:

$$\begin{aligned} H_{m_0} &= 4\sqrt{m_0} \\ H_{rms} &= \sqrt{8\, m_0} \\ H_{1/10} &= 5.091\sqrt{m_0} \end{aligned} \tag{14}$$

The narrowness of a spectrum defined by the spectral width, ν, range from 0 to 1, and are expressed as (Longuet-Higgins 1975):

$$\nu = \sqrt{\frac{m_0 m_2}{m_1^2} - 1} \tag{15}$$

when $v \rightarrow 0$ then all wave energy is concentrated in a single frequency. On the contrary, v increases when wave energy is broadly distributed among frequencies. The spectral peakedness parameter, Q_p, defines the sharpness of a spectrum and may be calculated by (Goda 1970):

$$Q_p = \frac{2}{m_0^2}\int_0^\infty f\, S^2(f)\, df \tag{16}$$

The values of Q_p are normally more than 1. High values of Q_p correspond to narrow band and sharply peaked spectra.

BOUNDARY CONDITIONS

Spatial boundary conditions have been divided into five locations: the rigid bottom of the mud layer (bed), the interface of plain water and mud flow, the free surface of water, the inlet, and the outlet boundaries (Hejazi et al. 2013). For simulating regular wave propagation, a horizontal velocity distribution, according to wave characteristics, is imposed at the left boundary to generate the corresponding wave:

$$u(t) = 2\pi\, a_w\, f\, \frac{\cosh kz}{\sinh kd_w}\sin(2\pi\, f\, t) \tag{17}$$

where a_w is the wave amplitude at water surface, d_w is the water depth and z is the elevation from the rigid bed. According to the irregular wave concept of Longet-Higgins et al. (1961), the water surface elevation can be described by Eq. 9, therefore the horizontal velocity distribution at the inlet to generate an irregular wave is defined by Eq. 19 as follows:

$$u(t) = \sum_{n=1}^{\infty} 2\pi\, a_{wn}\, f_n\, \frac{\cosh k_n z}{\sinh k_n d_w}\sin(2\pi\, f\, t + \varepsilon_n) \tag{18}$$

where $a_{wn} = \sqrt{2\,S(f_n)\Delta f}$ and the wave numbers, k_n, are computed from the corresponding frequency ω_n using a dispersion relationship. The wave energy density, $S(f)$, may be calculated from standard wave spectral formulations used for laboratory modeling. The mathematical formulation for JONSWAP, Pierson-Moskowitz, and Neumann spectra are respectively as follows:

$$S(f) = 0.2044 H_s^2 \frac{f_p^4}{f^5} \exp\left[-1.25\left(\frac{f_p}{f}\right)^5\right] \gamma^{\exp\left[\frac{(f-f_p)^2}{2\sigma^2 f_p^2}\right]} \tag{19}$$

$$S(f) = 0.313 H_s^2 \frac{f_p^4}{f^5} \exp\left[-1.25\left(\frac{f_p}{f}\right)^4\right] \tag{20}$$

$$S(f) = 1.466 H_s^2 \frac{f_p^5}{f^6} \exp\left[-3.\left(\frac{f_p}{f}\right)^2\right] \tag{21}$$

where H_s is the significant wave height, γ is the peak enhancement factor which is taken 3.3, f_p is the peak frequency, and σ is a function of wave frequency defined by $\sigma = 0.07$ for $f < f_p$, while $\sigma = 0.09$ for $f \geq f_p$.

NUMERICAL METHOD

The numerical model uses a structured non-orthogonal curvilinear staggered mesh and is capable of simulating non-homogeneous, stratified flow fields. Projection method has been deployed for solving the non-hydrostatic Reynolds-averaged Navier–Stokes equations. Using finite volume method in the ALE system, the newly updated free surface is determined purely by the Lagrangian method, and by the velocity of the fluid particles at the free surface, while the nodes in the interior of the domain are displaced in an arbitrary prescribed manner to be redistributed to avoid mesh crossing. To solve the set of the equations, in the first step the pressure gradient terms are omitted from the momentum equations, and the unsteady equations which include the advective and diffusive terms, are advanced in time to obtain a provisional velocity field. In the second step the provisional velocity is corrected by accounting for the pressure gradient and the continuity constraint. The water elevation is computed through the solution of the free surface equation. The interface elevation is obtained by the application of the integration of the continuity equation over the mud layer depth, and the kinematic boundary conditions at bed and interface. The mesh is re-generated at each time step in mud and water layers independently. The apparent viscosity of fluid mud, the expression in bracket in Eq. 8, has been calculated explicitly, based on the values of velocity field at the previous time step.

MODEL VALIDATIONS

Two examples of free-surface flow problems with significant non-hydrostatic pressure have been chosen to evaluate the numerical model. The first example is a periodic wave propagating over a submerged bar. This test also confirms the capability of the model to simulate free-surface flows interacting with uneven bottoms. In the second test for propagation of an irregular wave, variation of significant wave heights has been considered. Finally a two-layer system of water and fluid mud has been used to investigate irregular wave-mud interaction. For this test, variations of different parameters of spectral characteristics along the mud layer have been evaluated.

Periodic Progressive Wave Over a Submerged Bar

The objective of this test is to confirm the capability of the model to simulate the relatively strong interaction between non-linear wave and uneven bottom. The experimental set-up conducted by Beji and Battijes (1994) has been applied for the numerical simulation. The geometry for the numerical computation is depicted in Fig. 3. At the inflow boundary a progressive wave with a wave height of H_0 = 0.5 m and a period of T_0 = 2 s was specified. The computational domain was discretized by grids of Δx = 0.04 m in the x-direction, and the depth of the domain was divided into 20 layers. A time step of Δt = 0.01 s was chosen. The comparisons between the numerical simulations and the experimental data, for the free-surface elevation at seven wave gauge locations, are shown in Fig. 4. It is evident that the wave shape is gradually changing as wave passes over the submerged bar. At the front slope, as

water depth becomes shallower, the wave height was increased, the wave crest has become sharper, the wave trough has become flatter and the nonlinearity of wave was enhanced, and due to the nonlinear effect, the wave energy is transferred from low frequency to high frequency. When wave passes over the top of the bar, the nonlinearity effect weakens as water depth becomes larger. Because wave phase velocity varies with frequency in deep water, the high frequency wave propagates slower and is gradually separated from the main wave as a secondary wave. The complex wave phenomenon has been well simulated by the numerical model, which proves the ability of the model for efficiently simulating wave propagation.

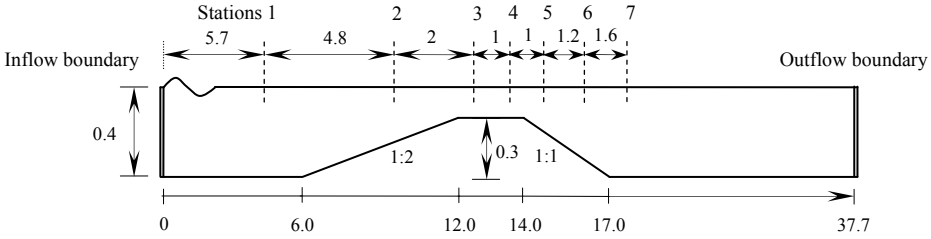

Figure 3. Sketch of the geometry for periodic wave propagation over a submerged bar. Dimensions are in meter.

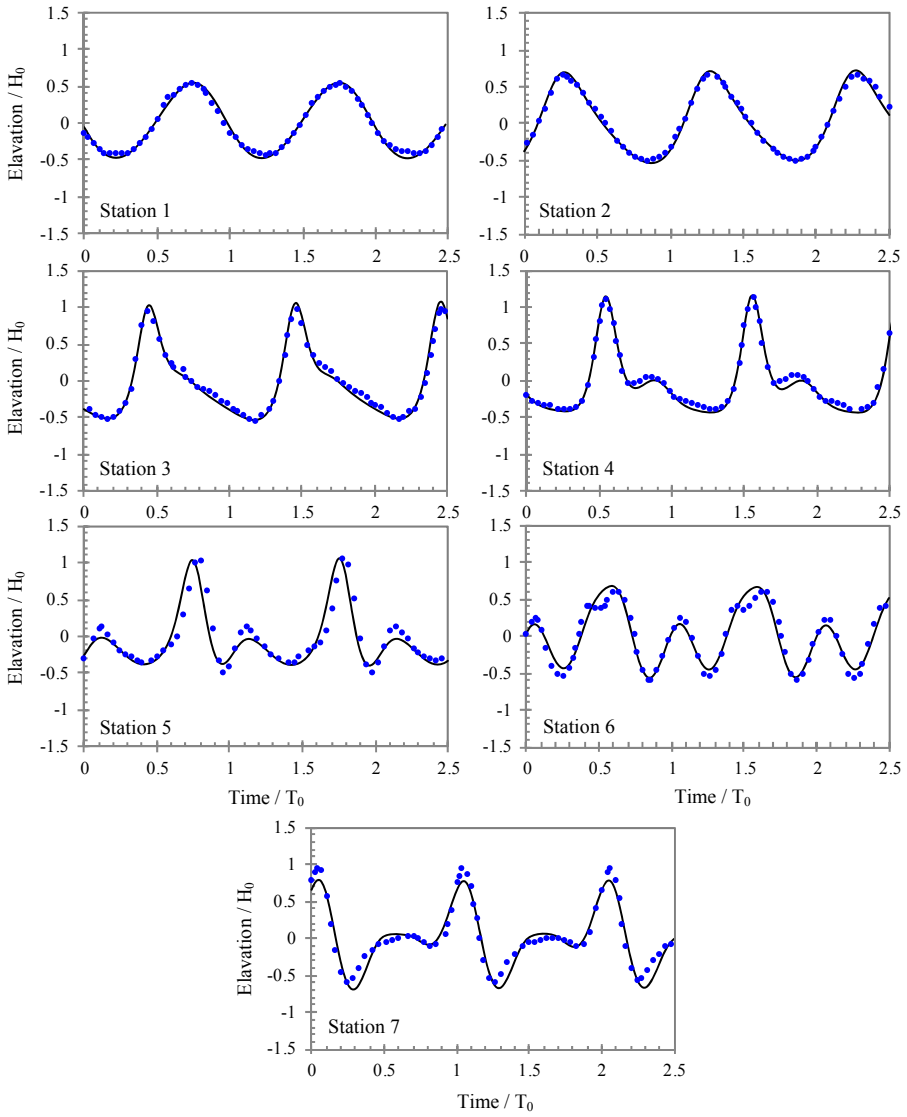

Figure 4. Comparisons of the free-surface elevation between numerical results (solid lines) and experimental data (circles) at seven wave gauge stations.

Irregular Wave Propagation in a Constant Water Depth

The second test simulates the irregular wave propagating from the left to the right along a 75 m long, 2.5 m deep wave flume based on experimental setup of Goullet and Choi (2011), with the initial water elevation being set equal to zero. The significant wave height, H_s, of 0.1 m and peak frequency, T_p, of 1 s have been applied as input to JONSWAP spectrum with the peak enhancement factor, γ, of 3.3. 10 wave probes were equally spaced at 1.2 m intervals where the first wave gauge was located at 17.8 m away from the wave-maker. Space and time intervals and the number of computational layers are set to 0.08 m, 0.004 s and 30 respectively. Numerical predictions of the wave amplitude time series for 200 s are presented in Fig. 5 at the first and tenth wave gauges. The derived spectra of the predicted water surface elevations at the first and tenth wave gauges are plotted in Fig. 6. The discrepancy between these two spectra is quite small. Simulated values of significant wave height along the wave flume at ten wave gauges have been compared with experimental data of Goullet and Choi (2011) in Fig. 7. In spite of small variations, wave height remains almost constant along the flume.

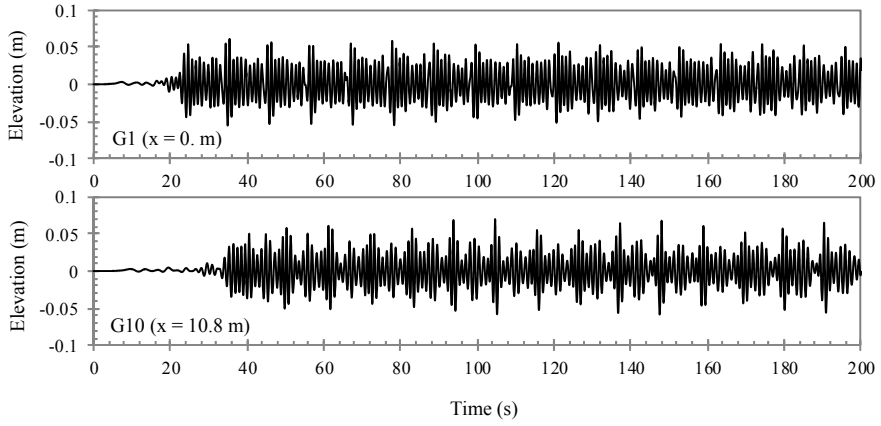

Figure 5. Numerical prediction of water surface elevations of random waves.

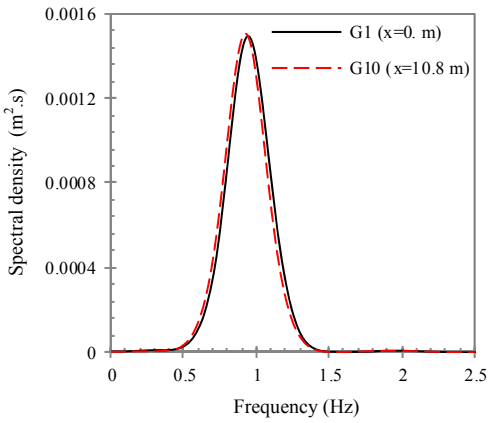

Figure 6. Comparison between numerical prediction of spectra at the first and tenth wave gauges.

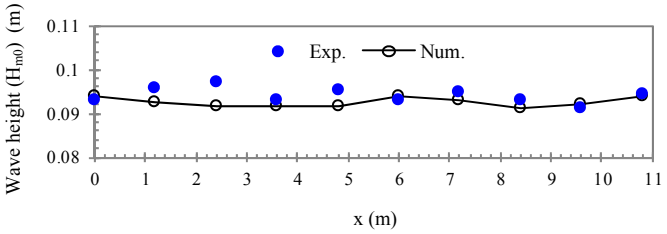

Figure 7. Comparison of predicted and measured values of H_{m0}.

Irregular Wave Propagation in a system of water and fluid mud

A series of laboratory experiments using commercial kaolinite were conducted by Samsami (2012) to investigate the irregularity effects and spectral shapes of waves traveling over fluid mud layers. The experiments were carried out in a flume with a length of 17 m. The flume was fitted with a false bed to accommodate the mud layer with a length of 9 m. The initial mud and water depth were 0.1 m and 0.2 m, respectively. Eight conductive wave gauges at equally spaced distances of 1.2 meter were simultaneously employed to measure rapid changes of surface water levels along the wave flume, where the first gauge measures the water elevation before the mud layer. Three various wave spectra of JONSWAP, Pierson-Moskowitz and Neumann with different wave heights and frequencies were employed. Five different incident wave conditions for JONSWAP (JT), Pierson-Moskowitz (PT) and Neumann (NT) test cases chosen for numerical simulations, are listed in Table 1. A Bingham plastic rheology according to Papanastasiou's relationship was assumed for the bottom fluid mud layer with τ_y = 14.83 N/m^2 and μ_B = 0.734 Pa.s, which was adopted from the laboratory rheological experiments of Samsami (2012). The density of mud was ρ_m = 1,350 kg/m^3, and the water density was taken 1,000 kg/m^3. Numerical parameters were set as Δx = 0.015 m and Δt = 0.0025 s, and the simulation time was set to 180 s. Water depth and the mud layer were divided into 16 and 8 layers respectively.

Fig. 8 represents the comparisons between the measured and simulated spectral density at wave gauges along the muddy bed for the test case JT1. The results indicate that the fluid mud bed absorbs the wave energy of wave spectra resulting to energy dissipation along the wave flume. Comparisons between the measured and simulated significant wave heights, H_{m_0}, along the mud layer for all test cases have been shown in Fig. 9. Also root-mean-square wave heights, H_{rms}, and the average of the highest 1/10 of the waves, $H_{1/10}$, have been plotted for the test case JT1. Table 1 tabulates the values of predicted and measured significant wave heights and the corresponding absolute percentage error (APE). The average of APE for all test cases is 7.33%. Fig. 10 shows the small discrepancies between the simulated and measured significant wave heights.

Comparison of the experimental data for the spectral bandwidth, v, at the end and the beginning of the mud section for all test cases reveal the slight increase of the spectral width parameter along the mud bed (Fig. 11), which can be related to different energy dissipation rates of irregular wave components that results to the unbalanced changes of spectral moments m_0, m_1 and m_2. Unlike this, the numerical prediction of the spectral bandwidth remains constant along the wave gauges as shown in Fig. 11. Significant wave height damping coefficients, k_i, have been calculated according to the exponential decay law, and are tabulated in Table 2. The predicted wave damping coefficients are greater than experimental values except in one test. Table 2 also contains the values of data scattering, R^2, of the numerical predictions and experiment data. The correlation between the predicted results of H_{m_0} is more than the measured data.

Comparisons of wave damping coefficient versus spectral peakedness parameter between measured and predicted values have been plotted in Fig. 12. In spite of differences between simulated and experimental values for wave damping coefficient and spectral peakedness parameter, it is observed that the wave dissipation on fluid mud layer generally increases with the increase of the spectral peakedness parameter. In other words, the narrow band and sharply peaked spectra traveling over muddy beds show higher energy dissipation rates.

Table 1. Comparisons of predicted and measured significant wave heights along the mud layer and the corresponding absolute percentage error.

Gauge No.	Test No. / T_p (s)														
	JT1 1.02			JT2 1.02			JT3 1.28			PT 1.02			NT 1.14		
	H_{m0} (m) × 10^{-2}			H_{m0} (m) × 10^{-2}			H_{m0} (m) × 10^{-2}			H_{m0} (m) × 10^{-2}			H_{m0} (m) × 10^{-2}		
	Exp.	Num.	APE(%)	Exp.	Num.	APE(%)	Exp.	Num.	APE(%)	Exp.	Num.	APE(%)	Exp.	Num.	APE(%)
G1	3.96	3.92	9.7	3.44	3.37	2.0	3.23	3.23	0.0	1.93	1.84	4.8	1.14	1.11	2.3
G2	3.51	3.61	2.9	2.63	3.19	21	3.11	3.28	5.5	1.71	1.77	3.4	1.06	1.09	2.5
G3	3.32	3.46	4.2	2.50	3.03	21	3.15	3.12	1.0	1.59	1.83	14	1.06	1.10	3.8
G4	3.36	3.31	1.5	2.38	2.95	23	2.88	2.79	3.1	1.62	1.73	6.5	1.06	1.04	1.7
G5	3.43	3.17	7.5	2.45	2.92	19	3.03	2.72	10	1.68	1.62	3.5	1.11	1.02	8.2
G6	3.20	3.06	4.4	2.35	2.79	18	3.02	2.76	8.6	1.59	1.61	1.0	1.07	1.02	4.7
G7	3.34	2.96	1.1	2.23	2.63	17	2.94	2.80	4.8	1.63	1.51	7.6	1.07	1.00	6.2
G8	3.10	2.96	4.6	2.27	2.48	9.3	2.81	2.73	2.8	1.51	1.60	5.6	1.04	0.94	9.7

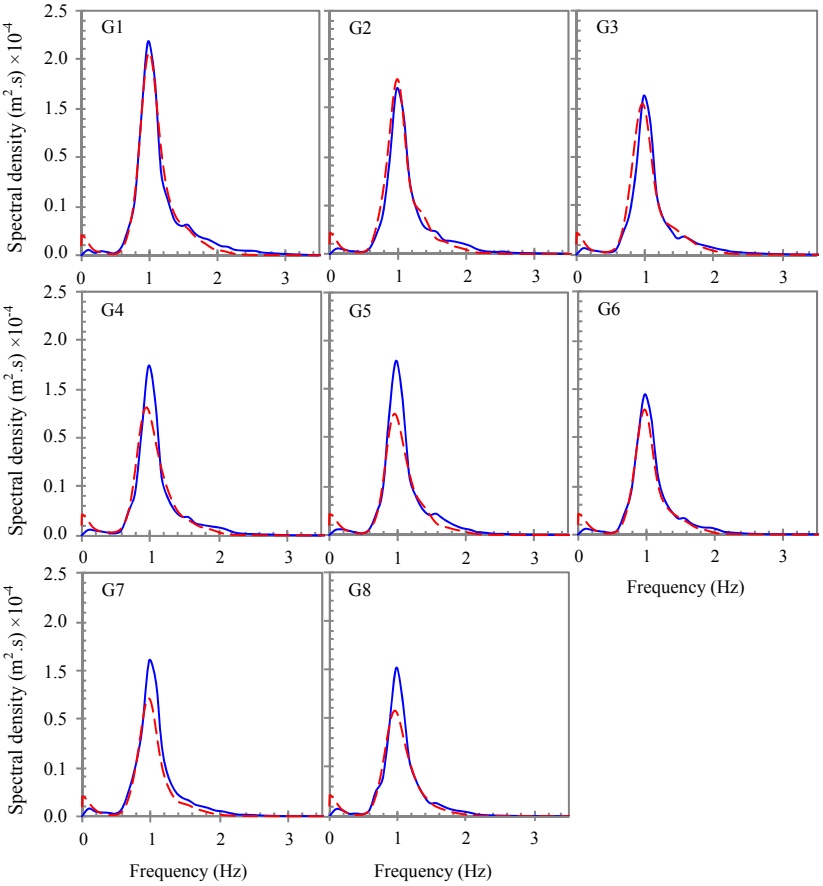

Figure 8. Comparisons of predicted wave spectra (dashed lines) against measured data (solid lines) (Test case JT1).

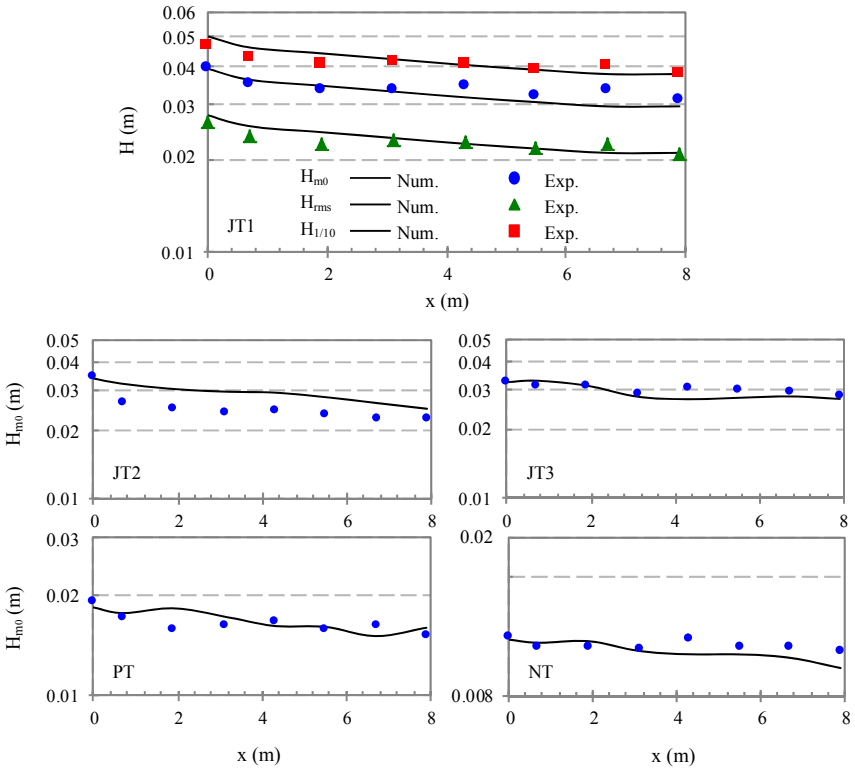

Figure 9. Comparisons of predicted and measured wave heights along the mud layer.

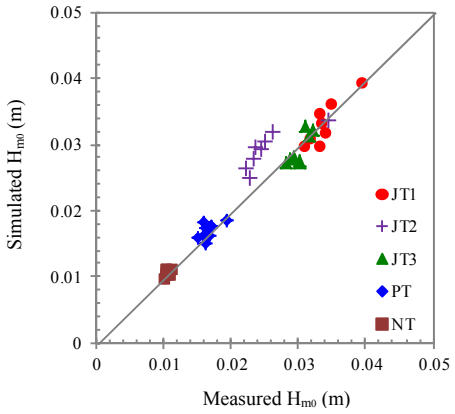

Figure 10. Comparisons of predicted and measured significant wave heights along the mud layer.

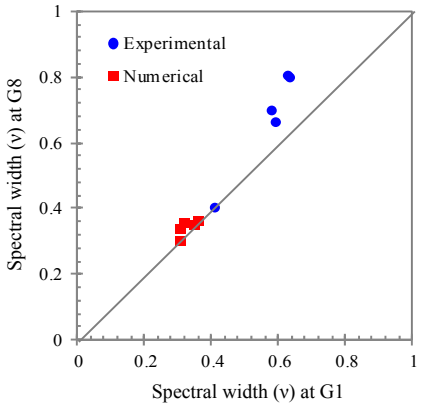

Figure 11. Spectral bandwidth parameter at gauge No. 1 versus gauge No. 8.

Table 2. Comparisons of predicted and measured wave damping coefficient and R^2.

Test No.	JT1		JT2		JT3		PT		NT	
	Exp.	Num.	Exp.	Num.	Exp.	Num.	Exp.	Num.	Exp.	Num.
k_i (m^{-1})	0.020	0.034	0.039	0.034	0.014	0.024	0.019	0.023	0.005	0.019
R^2	0.632	0.995	0.629	0.968	0.679	0.740	0.552	0.818	0.227	0.923

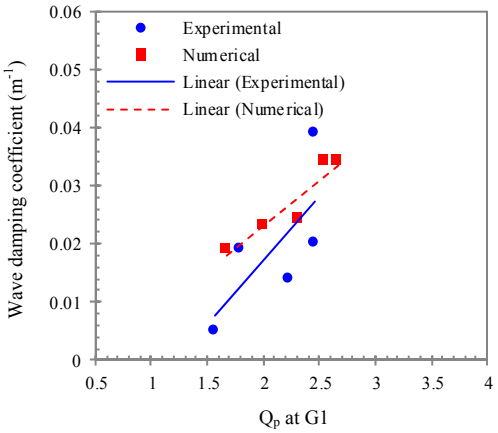

Figure 12. Spectral peakedness parameter versus wave height attenuation coefficient.

CONCLUSIONS

An ALE 2DV numerical model has been utilized to simulate the propagation of irregular waves in a system of water and Bingham fluid mud using wave spectra method. Firstly the model was validated by a series of free-surface flow tests with significant vertical accelerations, including a periodic wave propagation over a submerged bar and the irregular wave propagation in a constant water depth. Then the numerical tests have been conducted to confirm the ability of the numerical model for simulating irregular wave mud interaction. The conclusions are outlined as follows:

- Numerical predictions for periodic wave propagation over a bar indicate the capability of the model in simulating the interaction of non-linear waves with irregular and complicated bed geometry.
- Irregular wave propagation in water shows small variations of energy density and H_{m_0}.
- The wave attenuation along mud layer has been simulated by wave spectra method. Comparison of the predicted and measured energy density at eight locations along the flume shows good agreements.

- While the slope of wave attenuation for simulated H_{m_0}, H_{rms} and $H_{1/10}$ slightly fluctuates around the corresponding measured values, the predictions confirm the ability of the model in simulating the irregular wave propagation over the muddy bed.
- The comparisons between model predictions and measured data for H_{m_0} show fairly good agreement.
- The numerical model over-predicts the k_i values compared with the experimental-based data.
- Correlation between the predictions for H_{m_0} is closer than the measured data.
- The model predictions show an increasing trend of k_i versus increasing Q_p, similar to the experimental values. The increasing slope is milder in model predictions.

Overall, in spite of appropriate numerical results of significant wave height in comparison with measured values along the mud layer, the shape parameters of simulated spectra, i.e. v and Q_p, are not in good agreements with experimental-based data. This is due to the model inability in simulation of high frequency waves.

REFERENCES

Beji, S., and J.A. Battijes. 1994. Numerical simulation of non-linear waves propagation over a bar, *Coastal Engineering*, 23, 1-16.

De Boer, G.J., A.R. van Dongeren, and J.C. Winterwerp. 2009. *Wave damping by fluid mud*, Research Report No. Z4700/1200266.007, Deltares, 24 pp.

Goda, Y. 1970. *Numerical experiments on wave statistics with spectral simulation*, Rep. of the Port and Harbour Res. Inst. 57 pp.

Goda, Y. 2000. *Random seas and design of maritime structures*, World Scientific, Singapore, 443 pp.

Goullet, A., and W. Choi. 2011. A numerical and experimental study on the nonlinear evolution of long-crested irregular waves, *Physics of Fluids*, 23, 016601:1-15.

Hejazi, K., M. Soltanpour, and S. Sami. 2013. Numerical modeling of wave-mud interaction using projection method, *Ocean Dynamics*, 63, 1093-1111.

Kranenburg, W. 2008. *Modelling of wave damping by fluid mud; Derivation of a dispersion equation and energy dissipation term and implementation in SWAN*, MSc. Thesis, Delft University of Tech., 152 pp.

Longuet-Higgins M.S. 1975. On the joint distribution of the periods and amplitudes of sea waves, *Journal of Geophysical Research*, 80, 2688-2694.

Longet-Higgins, M.S., D.E. Cartwright, and N.D. Smith. 1961. Observation of the directional spectrum of sea waves using the motions of a floating buoy, *Proceedings of Conference on Ocean Wave Spectra*, 111-132.

Papanastasiou, T.C. 1987. Flow of materials with yield, *Journal of Rheology*, 31, 385-404.

Samsami, F. 2012. *Analysis of Wave Spectrum on Cohesive Beds*, Ph.D. Thesis, K.N.Toosi University of Tech., 274 pp.

Soltanpour, M., T. Shibayama, and Y. Masuya. 2007. Irregular wave attenuation and mud mass transport, *Coastal Engineering Journal*, 49, 127-148.

Zhang, Q.H., and Z.D. Zhao. 1999. Wave-mud interaction: wave attenuation and mud mass transport, *Proceedings of Coastal Sediments99*, 1867-1880.